Korean Membrane Journal
Vol. 8, No. 1 December, 2006, 1-12

A Pd Doped PVDF Hollow Fibre for the Dissolved Oxygen Removal Process

G. Barbieri[*,†], A. Brunetti[*,], F. Scura[*,**], F. Lentini[*,***], R. G. Agostino[***], M.-J. Kim[****], V. Formoso[***], E. Drioli[*,**], and K.-H. Lee[****]**

[*]National Research Council of Italy-Institute for Membrane Technology (ITM - CNR)Via Pietro BUCCI, The University of Calabria, cubo 17/C, 87030 Rende CS, Italy

[**]The University of Calabria - Department of Chemical Engineering and MaterialsVia Pietro BUCCI, cubo 44/A, 87030 Rende CS, Italy

[***]The University of Calabria, Department of PhysicsVia Pietro Bucci, cubo 31/C, 87030 Rende CS, Italy

[****]Membranes and Separation Research Center, Korea Research Institute of Chemical Technology (KRICT), P.O. BOX 107, Yuseong, Daejon 305-600, South Korea

(Received November 1, 2006, Accepted December 1, 2006)

Abstract: In semiconductor industries, dissolved oxygen is one of the most undesirable contaminants of ultrapure water. A method for dissolved oxygen removal (DOR) consists in the use of polymeric hollow fibres, loaded with a catalyst and fed with a reducing agent such as hydrogen. In this work, PVDF hollow fibres loaded with Pd were characterized by means of perporometry, scanning electron microscopy (SEM), energy dispersive X-ray (EDX). The hollow fibre analyzed shows a five-layer structure with remarkable morphological differences. An estimation of pore diameters and their distribution was performed giving a mean pore diameter of 100 nm. The permeance and selectivity of the fibres were measured using H_2, N_2, O_2 as single gases, at different operating conditions. An H_2 permeance of 37 mmol/m^{2}s was measured and H_2/O_2 and H_2/N_2 selectivities of *ca.* 3 were obtained. H_2 permeance was 1/3 when a water stream flows in the shell side. Catalytic fibrebehaviour was simulated using a mathematical model for a loop membrane reactor, considering only O_2 and H_2 diffusive transport inside the membrane and their catalytic reaction. Dimensionless parameters such as the Thiele modulus are employed to describe the system behaviour. The model agrees well with the experimental reaction data.

Keywords: *dissolved oxygen removal, PVDF hollow fibre, catalytic membrane modelling*

1. Introduction

Ultrapure water production is one of the key support services for the semiconductor, pharmaceutical, biotechnology, power and specialized chemical industries. Removal of dissolved oxygen (DOR) from water is an important step in this production process and can be achieved by either physical or chemical methods[1] Conventional physical methods such as thermal degassing, vacuum degassing or nitrogen bubble de-aeration have inherent drawbacks in terms of both operating costs and bulky construction. Also, with these physical methods, the reduction of dissolved oxygen concentration from a high ppm level down to a few ppm, [2,3] often required in the semiconductor industries for water cleaning, is difficult. Conventional chemical methods such as the addition of hydrazine or sodium sulphite, despite providing an alternative to physical methods are undesirable, owing to the toxicity or to the increase of the solid content, respectively. Reaction with a reducing agent such as hydrogen in the presence of a catalyst to form water is an attractive meth-

[†]Author for all correspondences
(e-mail : g.barbieri@itm.cnr.it)

od since it produces no by-product to contaminate the water. Kasama *et al.*, (1990)[2] have conducted a comprehensive study on DOR from water. Four different systems were considered in their study, namely nitrogen gas bubbling de-aeration, catalytic reaction and hybrid systems of both these methods where a hollow fibre membrane module with oxygen selective membranes was utilized as a degassing pre-treatment prior to the nitrogen gas bubbling de-aeration system and the catalytic reduction reaction, respectively. Their experimental results indicatethat the second hybrid system gave the best de-oxygenation results and DO levels between 3 and 5 ppb were achieved.

Tai *et al.* (1994)[4] also studied the removal of dissolved oxygen from water using membrane modules. Unlike the modules used by Kasama *et al.* (1990) where the membrane is a non-porous selective type, that used by Tai *et al.* (1994) containsa hydrophobic microporous membrane. Water containing saturated oxygen was fed into the fibre lumen, while the purified nitrogen acting as purge gas was introduced into the shell side. Therefore the removal of dissolved oxygen from water is achieved by fast mass transfer rather than selective permeation. The experimental hydrophobic membrane modules were capable of reducing the dissolved oxygen content in water to a level of around 8 ppm.

Different simulation works on DOR in both membrane and traditional reactors are present in the literature. Tan and Li[5] proposed a comparison between a hollow fibre membrane reactor and a tubular membrane reactor using H_2 as reducing agent. In the first case the Pd catalyst was packed in the void space of the shell reactor, whereas for the tubular membrane reactor, the catalyst was packed within the membrane tube. The 1-D models consider the H_2 permeation from gas phase toward the catalyst packed bed where a pseudo-homogeneous reaction takes place. Li *et al.*[6] proposed the simulation of a novel glass reactor for DOR from water. In this study, the hydrogen permeation from the shell side through the micro-porous glass tube has been employed for ultraviolet light catalysed reduction reaction.

Table 1. Operating Conditions of the Permeation Tests

Temperature, °C	Room Temperature
Retentate pressure	101~200 kPa
Permeate pressure	100 kPa
Pure gases	H_2, N_2, O_2
Feed flow rate	1~20 cm^3 (STP)/min
Water feed flow rate on the shell side ("Wet" mode)	10 mL/min

The objective of this work is the study of a Pd doped PVDF hollow fibre for the DOR. The Pd clusters on the PVDF surface act as catalyst for the reaction using hydrogen as reducing agent. Morphological and chemical characterizations were carried out in order to study the fibre structure. Gas permeation tests were also performed to identify thepermeation properties of the membrane such as permeance and selectivity. A mathematical model was developed to simulate dissolved oxygen removal by reduction reaction using the Pd-doped PVDF hollow fibre.

2. Materials and Methods

2.1. Experimental Setup

The single fibre was connected in a tubular nylon module with stainless steel connections. The permeation tests were carried out with single gases (H_2, N_2, O_2) using the pressure drop method. A pressure controller is used for the feed pressure, and the permeate stream was measured by means of a bubble soap flow meter. Hydrogen permeance was also measured feeding a water stream in co- and counter-current mode on the shell side. The operating conditions are reported in Table 1.

The tests on DOR by means of catalytic reaction were carried out in the experimental set-up described in Fig. 1. A flat PVDF porous membrane doped with different Pt or Pd loads is the core of the system. The oxygen contained in the water reacts with hydrogen

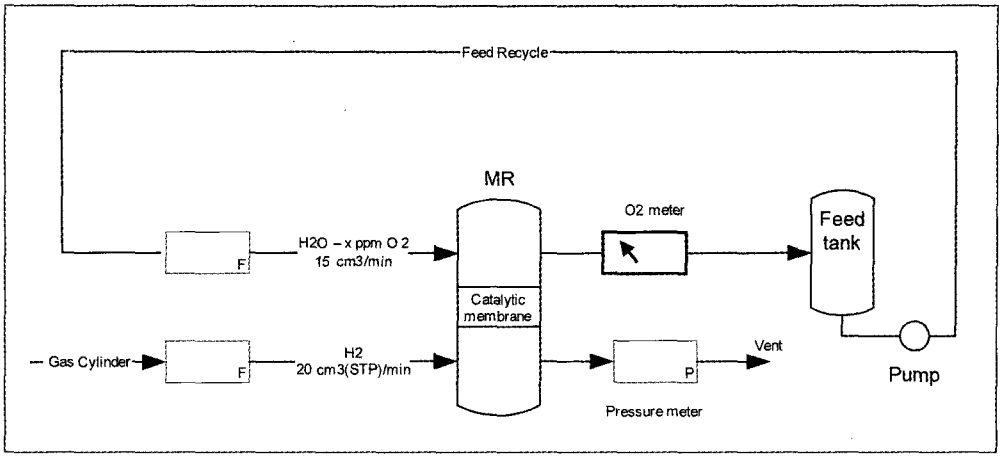

Fig. 1. Scheme of the experimental setup for DOR reaction using a catalytic membrane.

fed on the other membrane side. A fixed volume of water is continuously re-circulated and no input or output in this stream are present. The hydrogen is fed in largeexcess and at a constant pressure. The system can be considered as a "loop" reactor, since the O_2, being a limiting reactant, is re-circulated and the hydrogen is in large excess.

2.2. Mathematical Model

Fig. 2 reports a scheme of the experimental setup of Fig. 1 considering all the characteristics of the process. The fixed volume of water can be seen as a liquid "column" in contact with the catalytic membrane characterised by no gradient or a perfect mixing (owing to the re-circulation).

The "loop-reactor" must be considered as a batch system where the oxygen is reduced on the catalyticmembrane by the hydrogen present in a large excess. Therefore, a 1-D mathematical model for the simulation of the DOR was developed.

O_2 and H_2 are fed from the two different membrane sides (Fig. 3). The reaction slowness allows the external mass transport to be neglected (no water physical property changes occurs owing to the reaction). Therefore, the model considers only the diffusive transport inside the membrane of the two species and their catalytic reaction. The amount of low heat developed by the reaction (low initial O_2 concentration) compared to the high heat capacity of the liquid phase allows the system to be considered as isothermal and no energy balance is useful. The reaction has been considered as pseudo-homogeneous.

A 1-D, 2^{nd} order partial differential equations (PDEs) for the transient species diffusion and reaction inside the catalytic membrane layer are written. The dimensionless form of the mass balance equations is reported in Table 2 with the corresponding initial and boundary conditions (I.C. and B.C.).

An ordinary differential equation (ODE) expressing oxygen concentration evolution in the liquid bulk phase is used as the B.C.1 in the O_2 mass balance ($z=0$) for the membrane phase. This B.C. correlates the O_2 concentration in the liquid bulk phase to the diffusive flux at interface between the liquid and the membrane, expressing the overall O_2 mass balance in the system. B.C.2 expresses the absence of O_2 flux at the interface between the membrane and the gas phase side; no stripping effects by means of H_2 flow in the gas phase membrane side was considered.

H_2 concentration in the liquid bulk phase is null since the H_2 solubility constant is one order of magnitude lower than that of the O_2 (B.C. 1) and (B.C. 2) H_2 concentration in the water at the interface between the membrane and gas phase is at equilibrium.

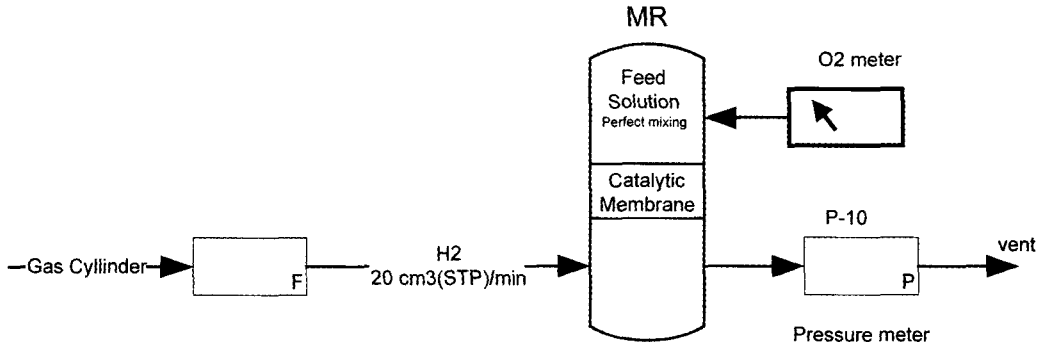

Fig. 2. Simplified scheme of the DOR process for the mathematical model.

Table 2. O_2 and H_2 transient Mass Balance Equations inside the Catalytic Layer of PVDF Membrane

Oxygen mass balance

$$\frac{\partial C^*_{O_2}}{\partial t^*} - \frac{\partial^2 C^*_{O_2}}{\partial z^{*2}} = -\Phi^2 R^*$$

$$I.C. \quad C^*_{O_2} = 0 \qquad (1)$$

$$B.C.1\ C^*_{O_2}(t)\Big|_{z^*=0} = \frac{C^0_{O_2} - \frac{A^{Membrane}}{V^{batch}} \int_0^t J_{O_2}\Big|_{z=0} dt}{C^0_{O_2}}$$

$$B.C.2\ \left.\frac{\partial C^*_{O_2}}{\partial z^*}\right|_{z^*=1} = 0$$

Hydrogen mass balance

$$\frac{\partial C^*_{H_2}}{\partial t^*} - \frac{\partial^2 C^*_{H_2}}{\partial z^{*2}} = -2\frac{D_{O_2,effective}}{D_{H_2,effective}}\Phi^2 R^*$$

$$I.C. \quad C^*_{H_2} = 0 \qquad (2)$$

$$B.C.1\ \left.\frac{\partial C^*_{H_2}}{\partial z^*}\right|_{z^*=0} = 0$$

$$B.C.2\ C^*_{H_2}\Big|_{z^*=1} = \frac{P_{H_2}}{K_{H_2}}$$

Table 3. Dimensionless Variables

Dimensionless concentration	$C^*_i = \frac{C_i}{C^0_{O_2}}$
Dimensionless catalytic layer thickness	$z^* = \frac{z}{\delta}$
Dimensionless time	$t^* = \frac{t}{\tau}$

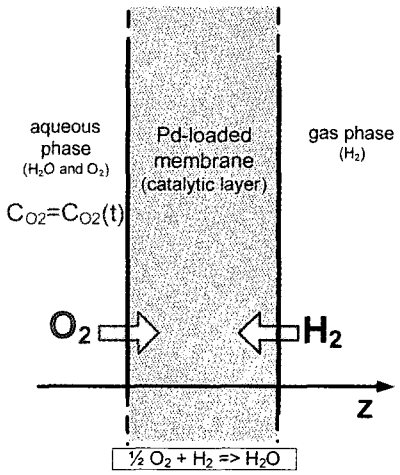

Fig. 3. Catalytic layer of PVDF membrane in which the DOR reaction takes place.

The I.C.s set to zero the initial concentration of both species inside the membrane.

Although there is no specific interest regarding the H_2 concentration profile inside the membrane, the H_2mass balance equation solution is required; for this reason the two PDEs must be solved simultaneously as a set. In fact, the expression of elementary reaction

Table 4. Operating Conditions of Simulations

Operating conditions	
Temperature, °C	25
Initial O_2 concentration, ppm	8.3
H_2 partial pressure, kPa	50:100:200
Membrane characteristics	
Catalytic membrane layer thickness, δ, nm	20
Membrane porosity, ε, -	0.3
Membrane area, $A^{Membrane}$, cm^2	70
Volume of liquid phase, V^{batch}, L	2
Physical parameters	
O_2 diffusivity in water, D_{O2}, m^2/min	1.446×10^{-7}
H_2 diffusivity in water, D_{H2}, m^2/min	2.06×10^{-7}
O_2 *Henry*'s constant K_{O2}, atm m^3/mol	7.884×10^{5}
H_2 *Henry*'s constant K_{H2}, atm m^3/mol	1.273×10^{6}

rete depends also on the H_2 concentration. The considered model for the O_2 reduction reaction rate is:

$$R = kC_{O_2}\left(C_{H_2}\right)^2 \tag{3}$$

In the *mass* balance equations Φ is the *Thiele modulus* ($\Phi^2 = \frac{k\left(\delta C^0_{O_2}\right)^2}{D_{O_2,effective}}$). It is the ratio of the reaction rate to the diffusion rate [7] inside the porous medium.

The definition of dimensionless variables employed in the simulations are reported in Table 3.

Table 5. Geometric Characteristics

Outer diameter	0.6 mm
Inner diameter	0.4 mm
Fibre length	150 mm
Separative layer thickness	20 μm

Where C^0_{O2} is the dissolved O_2 equilibrium value, δ isthe thickness of the membrane catalytic layer and τ is the characteristic time ($\tau = \frac{\delta^2}{D_{O_2,effective}}$).

Table 4 reports the operating conditions and the parameter values employed in the reaction tests.

3. Results and Discussion

3.1. PVDF Hollow Fibre Characterization

The PVDF hollow fibres loaded with Pd were characterized in terms of perporometry, morphology by scanning electron microscopy (SEM), composition profiles by energy dispersive X-ray (EDX) analyses. The instrument (SEM-EDAX) used for the characterization allows the chemical and morphological analysis to be performed simultaneously. High vacuum (10^{-7} mbar) and low vacuum (0.40 mbar) modes at different prime energy were used during the characterization.

Table 5 reports the geometric characteristics of the Pd-doped PVDF hollow fibres.

The fibre cross-section is shown in Fig. 4 for three different magnitudes of resolution. The analyzed hol-

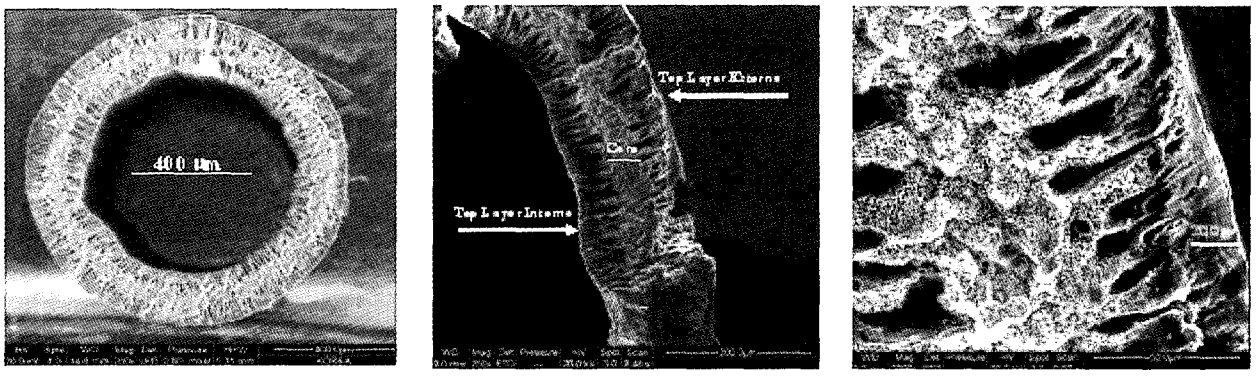

a) Mag. 200x b) Mag 250x c) Mag 2,000x

Fig. 4. SEM images of PVDF hollow fibre cross section.

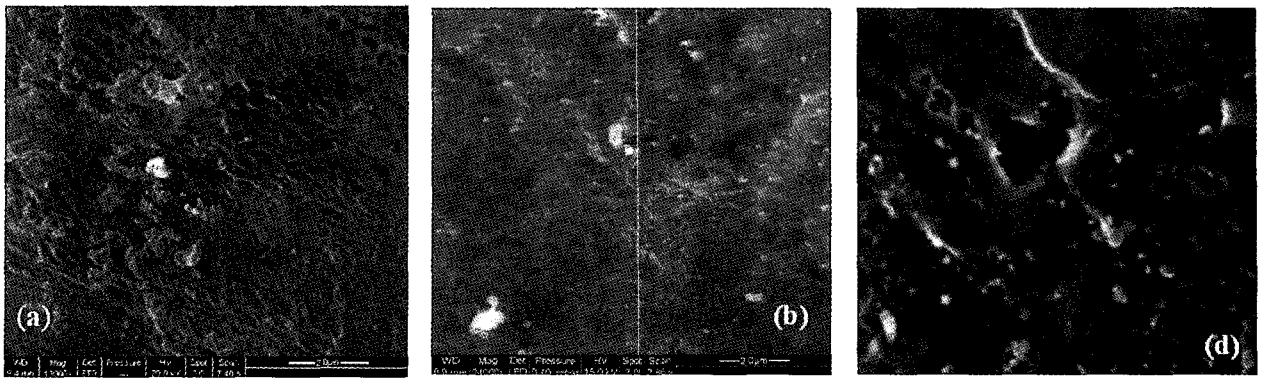

a) Mag 4.000x b) Mag 13.000x c) Mag 200.000x

Fig. 5. PVDF hollow fibre: SEM images of external top layer for different magnitudes.

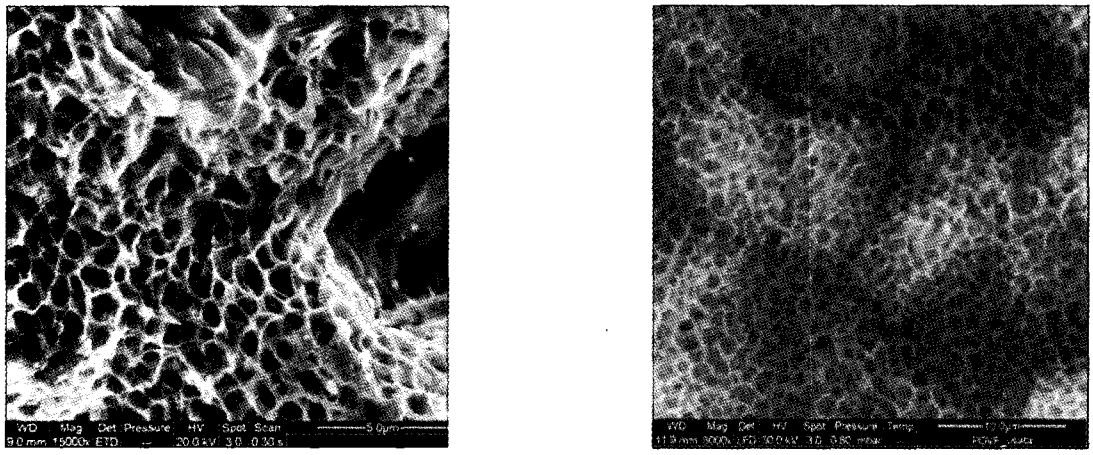

a) Mag. 15,000x b) Mag. 8,000x

Fig. 6. PVDF hollow fibre core: SEM images of cross-section (a) and longitudinal section (b).

low fibre shows a five-layer structure with remarkable morphological differences, specifically concerning the interfacial layer thicknesses and the Pd-dispersed percentage:

1) External Top-layer
2) Connection layer between external layer and core
3) Core
4) Connection layer between core and internal surface
5) Internal layer

Long channels with a length of ca. 25 microns and 10 microns of average diameter, distributed in a regular way, are present in the connecting layers between external layers and core (Fig. 4c). The same structure is shown by the connection layer core-internal surface.

A relevant difference among the morphology of the five layers can be shown by increasing the photo resolution (Fig. 4a-b). In particular, the external top layer seem to be almost dense and uniformly deposited on the connection layer with ca. 20 microns core.

The external top layer (Fig. 5) showed a homogenous and dense morphology, with ca. 18% porosity not uniformly distributed, with a pore size of ca. 100 nm. Furthermore, an absence of interconnectivity among the Pd grains in the form of unconnected clusters with a medium diameter of 20 nm, was confirmed by SEM and also conductivity tests which revealed an electric

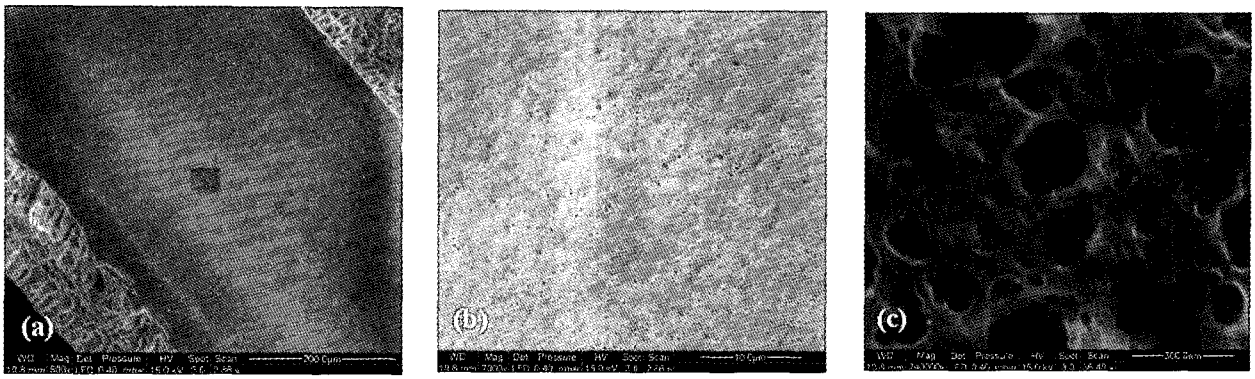

a) Mag 5.00x b) Mag 7.000x c) Mag 240.000x

Fig. 7. PVDF hollow fibre: SEM images of internal top layer for different magnitudes.

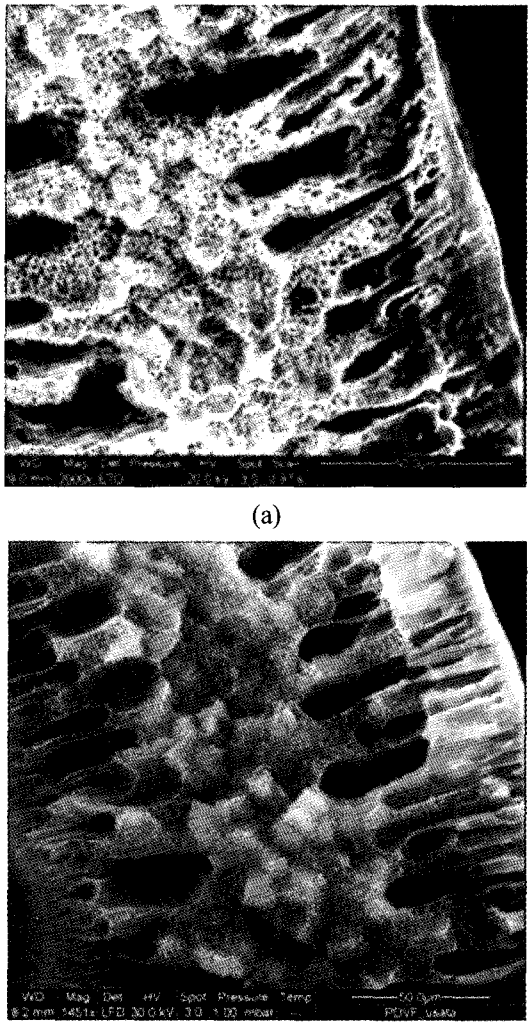

(a)

(b)

Fig. 8. PVDF hollow fibre: SEM images of cross-section before (a) and after (b) the permeation tests.

Table 6. Pd Doped PVDF Hollow Fibre. Chemical Composition of External Surface

Zoom / Mag		Highest 240,000x	Very High 200,000x	High 25,000x
Atomic %	C	$75.98_{\pm 0.2}$	$69.02_{\pm 0.4}$	$76.37_{\pm 0.4}$
	F	$18.97_{\pm 0.05}$	$24.63_{\pm 0.2}$	$15.85_{\pm 0.1}$
	O	$4.47_{\pm 0.04}$	$6.09_{\pm 0.1}$	$7.61_{\pm 0.1}$
	Pd	$\mathbf{0.13_{\pm 0.004}}$	$\mathbf{0.04_{\pm 0.003}}$	$\mathbf{0.02_{\pm 0.01}}$
	S	$0.10_{\pm 0.005}$		
	Na	$0.12_{\pm 0.01}$	$0.18_{\pm 0.02}$	$0.04_{\pm 0.02}$
	Ca	$0.07_{\pm 0.006}$	$0.02_{\pm 0.003}$	$0.02_{\pm 0.01}$
	Cl	$0.07_{\pm 0.05}$		$0.03_{\pm 0.01}$
	K	$0.04_{\pm 0.006}$		
	Si	$0.03_{\pm 0.005}$		
	Al	$0.02_{\pm 0.006}$	$0.04_{\pm 0.01}$	$0.04_{\pm 0.02}$
	Pores	Visible	Invisible	

resistance over 210 Ωm[8].

The core structure shows a sponge-like matrix with many cavities and a high porosity. However, comparing the longitudinal section (Fig. 6a) and the cross-section (Fig. 6b) no connection among the pores and long-distance orientation order are observed. The internal surface presented a different morphology with respect to the external surface. It shows a porosity of ca. 40%, with 100 nm of pore diameter. Furthermore the separative layer is a few microns thick, thus thinner than the external surface and no Pd clusters were observed by means of SEM photo also at a high

resolution.

A new morphological characterization of the fibre was carried out in order to evaluate the eventual changes in the structure owing to the testing after the permeation tests with pure gases also in the presence of water. No structural changes were observed in the fibre morphology (Fig. 8) from the comparison of the SEM photos obtained beforeand after the permeation tests. The connecting layer between the core and the top layers showed the same cylindrical channels, unchanged both in shape and in dimension.

A chemical analysis along a scan-line was performed in order to know the spatial distribution of the chemical elements (in particular Pd) along the crosssection.

Table 6 reports the chemical composition of the hollow fibre external surface obtained by means of EDAX. The presence of Pd is observed at all the image resolutions investigated[9].

An empirical formula was used to quantify the Pd amount on the external surface of the membrane. It allows the penetration distance of the primary bundle electrons to be calculated. The mean free path (λ_e) of a electron bundle can be calculated by means of the following relation:

$$\lambda_e = 538 \cdot d \cdot E_{beam}^{-2} + 0.13(d^3 E_{beam})^{0.5} \quad (4)$$

Where d corresponds to the distance between the first close atoms and the kinetic energy of the electrons bundle. The relation (4) is based on the hypothesis, supported by the chemical analysis, that the Pd is present only on the external surface of the fibre. The mean Pd cluster dimension was estimated around 15 nm, as found in the SEM photo, and the atomic distribution assumed 0.13% from the EDAX tests. Therefore the real Pd atomic percentage on the external surface can be calculated as follows:

$$Pd_{\%Atomic} \cong Pd_{\%At} \frac{\lambda_{max}}{OD_{cluster}} \cong 0.13\% \cdot \frac{1000\ nm}{15\ nm} = 8.7\% \quad (5)$$

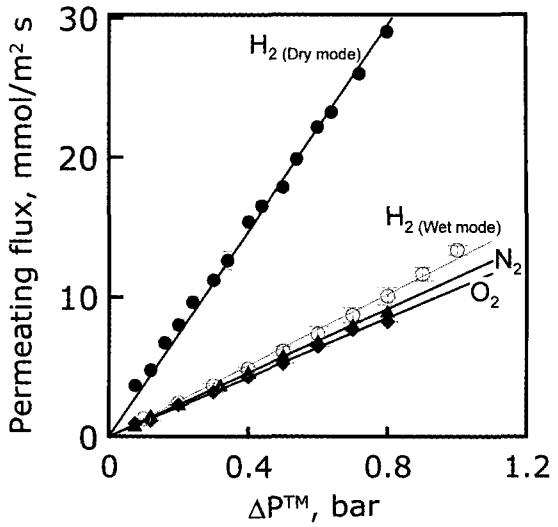

Fig. 9. Permeating flux as a function of driving force for H_2 (also in a presence of a water stream on permeate side), N_2, O_2. at room temperature.

Table 7. Permeance and Selectivitiesof Pd-doped PVDF Hollow Fibre

Permeance, mol/ m^2s Pa		
H_2	N_2	O_2
36.8	11.5	10.6
Selectivity, -		
H_2/N_2	H_2/O_2	N_2/O_2
3.2	3.2	1.1

No relevant amount of Pd was found in the chemical analysis of the internal surface, therefore, the membrane shows Pd-catalyst presence only on the external surface, with cluster shape and nanometric dimensions.

3.2. PVDF Hollow Fibre-Permeation Tests

Fig. 9 shows the results of the permeation tests carried out with N_2, O_2 and H_2 as single gases and, for the latter, also in wet mode, feeding water on the shell side. Specifically, the permeating fluxes of N_2, O_2 and H_2 show a linear dependence on the driving force in all the feed pressure ranges considered.

The permeance values obtained with dry tests are very high for all the gases considered, even if a selectivity of ca. 3 for H_2 with respect to the other gases

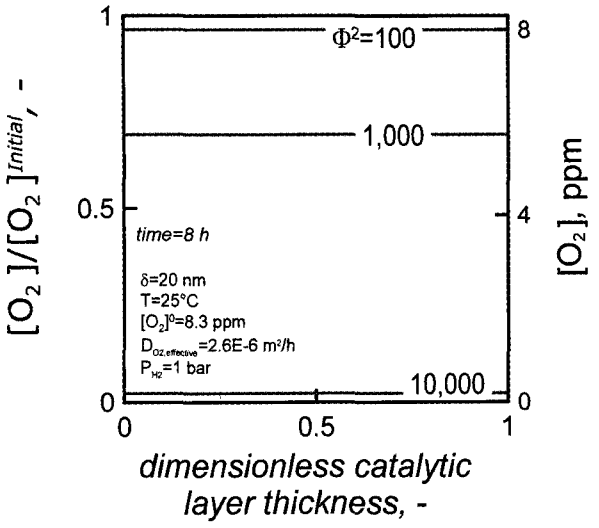

Fig. 10. Dimensionless oxygen concentration inside the catalytic layer of the membrane as a function of dimensionless catalytic layer thickness for different Thiele modulus, Φ^2.

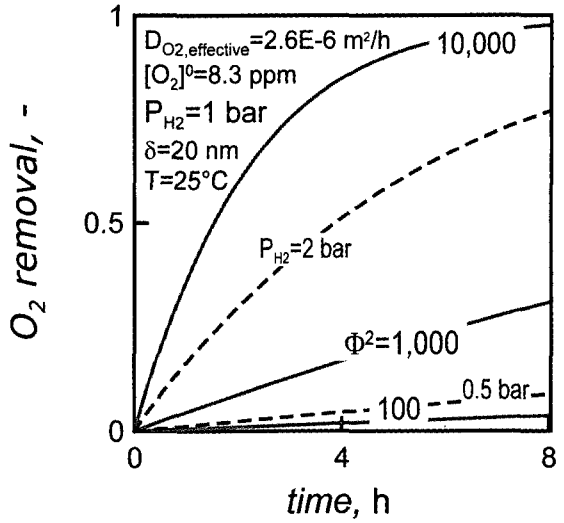

Fig. 11. Dissolved oxygen conversion in aqueous phase as a function of reaction time for different *Thiele* modulus, Φ and 100 kPa of H_2 partial pressure (continuous lines) and at a H_2 partial pressure of 200 kPa for Φ_2=1,000 (dashed lines).

is observed. Furthermore, the H_2 permeance value obtained in the wet tests is reduced by 60% with respect to the permeance in dry mode. No significant differences have been registered feeding the water in the shell side in co-current and counter-current configuration, in the ranged feed flow rate considered in the experiments.

3.3. DOR Reaction Simulation

The integration of mass balance equations gives the O_2 and H_2 profiles insidethe catalytic layer of the membrane during the time-evolution. In addition, also the evolution of O_2 concentration in the liquid bulk of the batch system can be obtained. Since the only parameter appearing in the equations is the *Thiele modulus*, a parametric solution of mass balances with respect to Thiele modulus is proposed.

In Fig. 10 the dimensionless O_2 concentration inside the membrane as a function of the dimensionless catalytic layer thickness is reported, after 8 hours of reaction and 100 kPa of H_2 partial pressure in the gas phase membrane side. The O_2 concentration profile is flat for all the different investigated *Thiele modulus* owing to the higher diffusion rate with respect to the

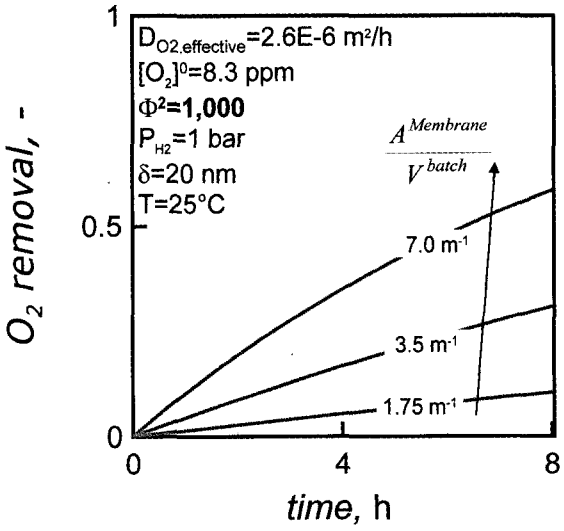

Fig. 12. Dissolved oxygen conversion in aqueous phase as a function of dimensionless reaction time, for different values of H_2 pressure in gas phase side, for a Φ_2=1,000.

reaction rate in the thinner membrane catalytic layer. In particular it is lower at a higher Thiele module value.

The removal of dissolved O_2 in the liquid bulk phase is an increasing function of reaction time (Fig. 11). The O_2 removal was evaluated by means of the

relationship:

$$O_2 \quad \text{Removal} = 1 - \frac{C^*_{O_2}}{C^*_{O_2,0}} \tag{6}$$

At a higher *Thiele modulus* a higher O_2 removal is reached. In the same figure the effect of different H_2 partial pressures in the gas phase side on the O_2 removal are reported, for a *Thiele modulus* equal to 1,000. A higher H_2 partial pressure (200 kPa) produces a faster reaction and, consequently, a greater O_2 removal.

Fig. 12 reports the O_2 removal as a function of reaction time for different ratios of the membrane area andbatch system volume, for Φ^2 equal to 1,000. Increasing this parameter a greater O_2 removal is achieved owing to the fact that a large catalytic membrane area promotes a greater O_2 flux inside the membrane and, consequently, a greater O_2 removal.

Fig. 13 reports a comparison between the simulation results and some experimental data. The O_2 removal measured for three different catalyst loads in the membrane and calculated by means of simulation for Φ^2 equal to 1,000 is reported as a function of reaction time. A good agreement is observed for the lower catalyst load.

4. Conclusions

The analyzed hollow fibre shows a five-layer structure with remarkable morphological differences specifically regarding interfacial layer thicknesses and Pd-dispersion. An external selective layer 20 microns thick with catalytic function was observed. An absence of interconnectivity among the Pd grains in the form of unconnected clusters with a medium diameter of 20 nm was confirmed by SEM and also conductivity tests which revealed an electric resistance over 210 Ωm. different porosities (18% and 40%) and thicknesses (20 and 1 microns) for the external and internal surfaces, respectively, having the same pore diameter of 100

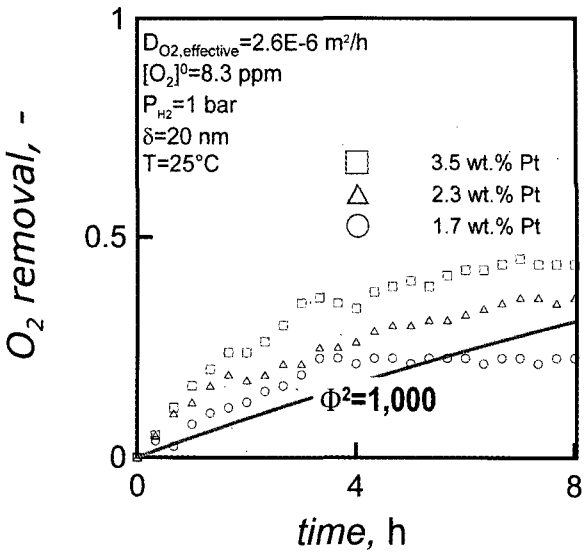

Fig. 13. Dissolved oxygen conversion in aqueous phase as a function of reaction time: comparison with experimental data (K. H. Lee *et al.*), at different % of catalyst load.

μm. Two layers 25 microns long and 10 microns wide connect the PVDF core and the internal and external surfaces. EDAX analysis shows the Pd only on the external surface.

An H_2permeance of 37 mmol/m^{2}s was measured and H_2/O_2 and H_2/N_2 selectivities of *ca.* 3 were obtained The H_2 permeance was 1/3 when a water stream flows in the shell side. However no fibreperformance dependence on the water flow rate and the water feed mode was observed.

The loop membrane reactor for the DOR reaction was simulated as a batch system with a catalytic membrane. A 1-D dimensionless mathematical model, consisting of O_2 and H_2 transient mass balances, allowed the DOR reaction to be simulated in the catalytic membrane. The species profile inside the membrane and the O_2 concentration evolution in the liquid phase are obtained in a wide range of operating conditions. Different *Thiele modulus* values and different H_2 partial pressures were investigated. A good agreement with experimental results in terms of O_2 removal was obtained for the lowest *Thiele modulus* value.

Acknowledgements

The "Ministero degli Affari Esteri, Direzione Generale per la Promozione e la Cooperazione Culturale" is gratefully acknowledged for the financial support for the bilateral project "Development of membranes and membrane processes for clean technologies with low environmental impact".

List of Symbols

A	Surface Area, m^2
C^*	*Dimensionless concentration,* -
C	Concentration, mol/L
d	First close atoms distance, m
D	Diffusivity, m^2/s
E	Activation energy, J/mol
E_{beam}	Kinetic energy of electrons bundle, eV/mol
F	Molar flow rate, mol/s
ID	Inner diameter, m
J	Permeating flux, mol/m^2 s
k	Kinetic constant, see related equation
K	Henry constant, -
L	Length, m
OD	Outer diameter, m
P	Pressure, Pa
Permeance	mol/m^2 s Pa
Q	Volumetric flow rate, m^3(STP)/s
R	Reaction rate, mol/m^3s
T	Temperature, °C or K
t	Time, h
thickness	Membrane thickness, m
V	Volume, m^3
X	Conversion, -
Y_i	Molar fraction of the species i^{th}, -
z	Axial coordinate, m

Greek letters

Π	Permeance, $mol/(m^2$ s Pa)
δ	Membrane thickness, m
ε	Porosity, -
τ	Characteristic time, s
λ_e	Electrons bundle mean free path

Subscripts

Effective	Porous membrane phase referred to
H2	Hydrogen referred to
O2	Hydrogen referred to

Superscripts

batch	Batch system referred to
Feed	Reaction side inlet stream
Membrane	Membrane phase
Permeate	Permeation side outlet stream
Retentate	Reaction side outlet stream
Sweep	Permeation side inlet stream

Acronyms

B.C.	Boundary Condition
I.C.	Initial Condition
MR	Membrane Reactor
PVDF	Polyvinildiflorure
STP	Standard temperature (25°C) and pressure (100 kPa)
ΔP	Permeation driving force, Pa

Dimensionless number

Φ	*Thiele* Modulus, -

References

1. K. Li, I. Chua, W. J. NG, and K. Teo, Removal of dissolved oxygen in ultrapure water production using a membrane reactor, Chemical Engineering Science (50) 3547-3556 (1995).
2. Y. Kasama, Y. Yagi, T. Imaoka, M. Kawakami, and T. Ohmi, Advanced D. I. water system with low dissolved oxygen for ULSI processing, Proceedings Institute of Environmental Science, pp. 344-349 (1990).
3. T. Imaoka, Y. Yagi, Y. Kasama, I. Sugiyama, T. Isagawa, and T. Ohmi, Advanced ultrapure water

systems for ULSI processing, in proceedings of the 10th Annual semiconductor Pure Water Conference, Santa Clara, CA, 26-28 February (Edited by M.K. Balaazs), pp. 128-146 (1991).

4. M. S. L. Tai, I. Chua, K. Li, W. J. Ng, and W. K. Teo, Removal of dissolved oxygen in ultrapure water production using microporous membrane modules, J. Membrane Sci. 87, 99-105 (1994).
5. X. Tan and K. Li, Investigation of novel membrane reactors for removal of dissolved oxygen from water, Chem. Eng. Sci 55, 1213-1224 (2000).
6. K. Li, T. Tan, V. Sinha, and W. K. Teo, Simulation of a novel glass reactor for dissolved oxygen removal from water, Wat. Res. 34, 2011-2024 (2000).
7. J. E. Bailey and D. F. Ollis, Biochemical Engineering Fundamentals, second edition 1977 by McGraw-Hill Inc., p. 212
8. G. Barbieri, A. Brunetti, F. Scura, F. Lentini, R. G. Agostino, M.-J. Kim, V. Formoso, E. Drioli, and K.-H. Lee, A Pd doped PVDF hollow fiber for the dissolved oxygen removal process, the 5th Italy-Korea workshop on "Membranes and membrane processes for a clean environment" (2006).
9. G. Barbieri, A. Brunetti, F. Lentini, R. G. Agostino, M. J. Kim, V. Formoso, E. Drioli, and K. H. Lee, Characterization and testing of Pd-doped PVDF hollow fibers for dissolved oxygen removal, E.C.I. Conference on Advanced Membrane Technology III: Membrane Engineering for Process Intensification (2006).